J. Fluid Mech. (1995), *vol.* 284, *pp.* 257–274

Gas flow in micro-channels

By JOHN C. HARLEY[1], YUFENG HUANG[1], HAIM H. BAU[1] AND JAY N. ZEMEL[2]

[1] Department of Mechanical Engineering and Applied Mechanics, University of Pennsylvania, Philadelphia, PA 19104-6315, USA

[2] Department of Electrical Engineering, University of Pennsylvania, Philadelphia, PA 19104-6315, USA

(Received 18 February 1993 and in revised form 2 September 1994)

An experimental and theoretical investigation of low Reynolds number, high subsonic Mach number, compressible gas flow in channels is presented. Nitrogen, helium, and argon gases were used. The channels were microfabricated on silicon wafers and were typically 100 μm wide, 10^4 μm long, and ranged in depth from 0.5 to 20 μm. The Knudsen number ranged from 10^{-3} to 0.4. The measured friction factor was in good agreement with theoretical predictions assuming isothermal, locally fully developed, first-order, slip flow.

1. Introduction

Micromechanics is a rapidly emerging technology in which micron-scaled devices are constructed using photolithographic methods similar to those employed to fabricate integrated circuits. Microfabricated channels may be used for integrated cooling of electronic circuits (Tuckerman 1984); Joule–Thomson cryo-coolers for infra-red detectors and diode lasers (Wu & Little 1983); miniature gas chromatographs built on single silicon wafers (Terry, Jerman & Angell 1979); and small, high-frequency fluidic control systems (Joyce 1983).

In order to design such devices effectively, it is necessary to establish the physical laws governing gas flow in small conduits. Among other things, such flow may differ from its macroscopic counterpart in that relatively high, subsonic Mach (M) numbers may be maintained concurrently with low Reynolds (Re) numbers, the surface area to volume ratio is huge, $O(10^6\ \mathrm{m^2/m^3})$, the fabrication process may lead to a relatively large degree of surface roughness, and non-continuum effects may occur at pressures above one atmosphere.

The prior studies which are most closely related to our work are those of Keenan & Neuman (1946), Shapiro (1953), Ebert & Sparrow (1965), Sreekanth (1968), Wu & Little (1983), Prud'homme, Chapman & Bowen (1986), van den Berg, ten Seldam & van der Gulik (1993*a*, *b*), and Choi, Barron & Warrington (1991). Keenan & Neumann (1946) and Shapiro (1953) reported on experimental work in which the friction factor for fully developed, continuum, adiabatic compressible gas flow ($M = 0.27$ to 3.87) in tubes ranging in diameter from 1 to 2 cm was approximately the same as the friction factor for incompressible flow with a comparable Reynolds number.

Sreekanth (1968) examined the flow of rarefied gases in 2 in. diameter tubes under large pressure gradients and Knudsen (Kn) numbers up to 0.265. For $Kn < 0.13$, his experimental results agreed well with theoretical predictions assuming a single coefficient wall slip model, and isothermal, locally fully developed flow. In contrast, Choi *et al.* (1991) measured a friction factor 17% below theoretical predictions for

nitrogen flow in circular channels with diameters smaller than 10 μm. Our estimate of the *Kn* number in their experiments suggest that such a deviation cannot be explained by non-continuum effects.

Wu & Little (1983) measured friction factors experimentally for both laminar and turbulent gas flow in miniature conduits etched in silicon and in glass. They observed friction factors larger than predicted by established correlations and a transition to turbulence at Reynolds numbers as low as 400. They attributed their anomalous results to the very high degree of surface roughness of some of their channels and to uncertainty in the determination of the dimensions of their channels. Part of the discrepancy may also be due to their comparison of experimental data for trapezoidal conduits with correlations established for pipes with a circular cross-section.

Surprisingly, there are only a few theoretical studies addressing compressible, laminar flow in uniform conduits. Prud'homme *et al.* (1986) and van den Berg *et al.* (1993*a*, *b*) neglected the transverse velocity and used a perturbation expansion to solve the isothermal, compressible Navier–Stokes equations for laminar flow in a circular tube. For low Reynolds and Mach number flows, they obtained a 'locally self-similar' velocity profile.

In this paper, we present experimental data, analytical predictions, and numerical simulations of compressible channel flow. We measured the pressure drop for the flow of nitrogen, helium, and argon in minute channels microfabricated on silicon wafers using photolithographic techniques borrowed from the electronics industry. In order to obtain the friction factor from the pressure measurements, knowledge of the velocity profile was required. To obtain the velocity profile, we used the 'locally fully developed' approximation, which we verified by comparing theoretical predictions with results of direct numerical simulations. The numerical simulations also provided information on the transverse velocity and the temperature field. The objective of this paper is to determine the range of validity of established theory for microchannel flow. A partial account of the experimental results described here was presented by Pfahler *et al.* at the 1991 ASME Winter Annual Meeting.

2. Experimental apparatus and procedure

The experimental apparatus is described in figure 1. The apparatus consists of two parts: the test section (figure 2), and an adapter, associated plumbing, and instrumentation which facilitates flow supply into the test section and the measurement of pressures, temperatures, and flow rates.

The text section (figure 2) consists of a flow conduit micromachined in $\langle 100 \rangle$ silicon using standard planar photolithographic techniques (Jaeger 1988). The conduits were capped with Pyrex glass anodically bonded (Wallis 1970) to the silicon. The shallowest channels (< 1 μm depth), were plasma-etched and had a rectangular cross-section. The deeper channels were etched with an anisotropic etchant, KOH, resulting in a trapezoidal cross-section in which the $\langle 111 \rangle$ planes intersect the wafer surface at an angle of 54.74° (figure 2*c*). Typically, the channels were 10^4 μm long, 100 μm wide, and ranged from 0.5 μm to 20 μm in depth. The various channels used in our experiments and their dimensions are listed in table 1. At both ends of the conduit, holes were etched in the silicon to allow the fluid to enter and exit the conduit.

Precise knowledge of the dimensions of a channel is extremely important for the accurate evaluation of the frictional resistance to motion within the channel; therefore great care was exercised in measuring channel dimensions. Before we bonded the Pyrex cap, the depth of the channel was measured with an accuracy of $\pm 1\,\%$ using a surface

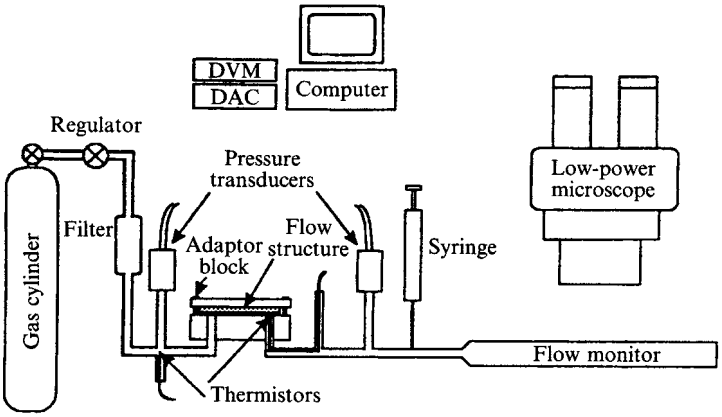

FIGURE 1. The experimental apparatus.

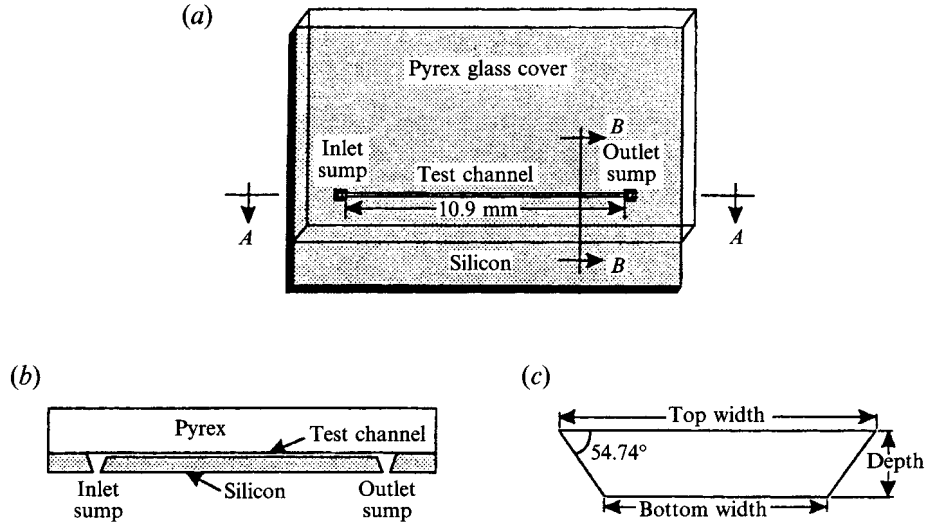

FIGURE 2. Views of a test channel microfabricated on a silicon wafer. (*a*) Top view. (*b*) Cross-section *A–A*. (*c*) Cross-section *B–B*.

Channel	Top width (μm)	Bottom width (μm)	Depth (μm)	Hydraulic diameter (μm)	Length $\times 10^3$ (μm)	Theoretical C, (Shah & London 1978)	Gases tested
JH6	96.6	96.9	0.51	1.01	10.9	95.13	N_2, He
V3	105.7	99.2	2.73	5.24	11.03	90.90	N_2
JP9	95.4	85.8	4.66	8.68	10.9	88.51	N_2, He
JH10	102.5	93.8	4.78	8.97	10.9	89.24	N_2
JH21	100.5	85.2	8.33	14.85	11.05	82.91	N_2, He, Ar
JH3	94.4	80.0	11.04	19.18	10.18	79.95	N_2, He, Ar
VJ27	99.3	75.5	15.98	26.03	11.08	74.10	N_2, He, Ar
JH5	246.8	220.3	19.79	35.91	10.18	84.94	N_2, He, Ar

TABLE 1. Microchannel specifications

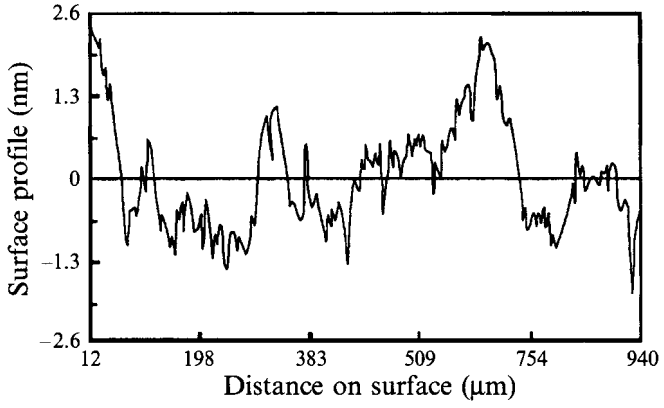

FIGURE 3. Laser interferometric microscope (WYKO) plot of the surface profile along a 0.5 μm deep channel. Peak–Valley = 4.88 nm; channel depth = 500 nm.

profilometer (Alpha-Step). These measurements were verified at the conclusion of the tests by cross-sectioning the wafers and examining them under a calibrated, scanning electron microscope. This 'postmortem' examination also assured that no change in dimensions occurred during the glass-cap bonding process and the high-pressure experiments. The width of the channels was measured optically, with a calibrated microscope reticle at 400×, allowing an accuracy of ±2%. The roughness of the channel was measured along its centre with both the surface profilometer and a laser interferometric microscope. Figure 3 depicts typical results of a surface interferometric measurement for a 0.5 μm deep channel with a roughness of about 1%.

The test section was pressure mounted in an adapter block (figure 1). O rings were used to prevent leakage at the contact points. The instrumentation necessary to monitor the inlet and exit pressures and temperatures as well as the flow rate was mounted outside the test section.

In the experiments, gas flowed from a regulated high-pressure cylinder, through a 0.5 μm filter, past a pressure transducer and a thermistor, into the adapter block, through the test section, back out to the adapter block, and through a flow-rate monitor. Downstream pressure and temperature were measured with another thermistor and pressure sensor (see figure 1). The volumetric flow rate was determined with a precision better than ±2.2% by timing the motion of an injected liquid meniscus through a tube which, depending on the flow rate, was either a precision bore capillary tube or a burette.

Owing to the unavailability of appropriate sensors which would allow *in situ* measurements, both temperatures and pressures were measured outside the test section. The difference between the upstream and downstream pressure measurements provided an estimate for the pressure drop inside the test section. The pressure losses outside the test section were estimated, in most cases, to be far less than 1% of the total pressure drop. In any event, data were excluded from consideration whenever the pressure drop in the supply lines was estimated to be more than 2.5% of the total pressure loss. The supply lines were in all cases at least an order of magnitude larger in diameter than the effective diameter of the test conduits. As a result, flow velocities in the supply lines were at least two orders of magnitude slower than those in the test conduits.

The temperatures were measured with minute thermistors. The gases entering the test section were at thermal equilibrium with the surroundings, and their temperature

was determined with an accuracy of ± 0.1 °C. Larger uncertainty was associated with the temperature measurement of the exiting gases. Because of the low specific heat and extremely low flow rate of the gas, conduction through the thermistor's leads could have caused a significant measurement error. Fortunately, even relatively large changes in exit temperature were estimated to have only a small effect on the determination of the friction factor.

Thermophysical properties of the gases used in the experiments were obtained from Touloukian, Saxena & Hestermans (1975).

3. A one-dimensional model for the evaluation of the friction factor

As the gas flows along the channel's length (x), its pressure decreases and its specific volume increases. To accommodate this increase in volume, the speed of the gas increases. The measured pressure drop, ΔP, along the channel's length, is caused by both shear and acceleration. In this section, we outline the procedure we used in order to subtract the contribution of acceleration from ΔP and obtain the average friction factor ($\bar{f}$).

The time-independent, one-dimensional, compressible, dimensionless, conservation equations for ideal gas flow in a uniform cross-section conduit are:

$$\rho\bar{u} = \text{const}, \tag{1}$$

$$\gamma^{-1}\,\mathrm{d}P + \mathrm{d}(\beta\rho\bar{u}^2) + \frac{\mu}{\mu_1}G^{-1}(\tfrac{4}{3}+\phi)\,\mathrm{d}\left(\frac{\mathrm{d}\bar{u}}{\mathrm{d}x}\right) + G^{-1}(\tfrac{1}{2}f)\,\rho\bar{u}^2\,\mathrm{d}x = 0, \tag{2}$$

$$\frac{4Nu}{Pr\,Re}(1-\theta_b)\,\mathrm{d}x = \mathrm{d}(\theta_b + \tfrac{1}{2}\alpha(\gamma-1)(\bar{u})^2), \tag{3}$$

$$P = \rho\theta. \tag{4}$$

In the above, $\bar{u} = (1/A)\int_A u\,\mathrm{d}A$ is the cross-sectionally averaged, axial velocity. u is the non-dimensional, local velocity normalized with the sound speed, $a_1 = (\gamma R T_1)^{1/2}$, evaluated at the channel's entrance temperature, T_1. A is the cross-sectional area of the channel. ρ is the non-dimensional gas density normalized with ρ_1. Subscripts 1 and 2 denote, respectively, conditions at the inlet and exit of the channel. P is the pressure normalized with the inlet pressure P_1. $\beta = (1/A\bar{u}^2)\int_A u^2\,\mathrm{d}A$ and $\alpha = (1/A\bar{u}^3)\int_A u^3\,\mathrm{d}A$. D_H is the hydraulic diameter which we use as the lengthscale. $Re = \rho\bar{u}D_H/\mu$ and $G = a_1 D_H \rho_1/\mu_1$ are the Reynolds and the acoustic Reynolds numbers, respectively. $f = 8\bar{\tau}_w/\rho\bar{u}^2$ is the Darcy friction factor. $\bar{\tau}_w$ is the average wall shear stress at location x along the length of the channel. μ is the shear viscosity. ϕ is the ratio between the bulk and shear viscosities. γ is the ratio of specific heats. θ is the temperature normalized with the inlet temperature, T_1. $Nu = hD_H/k$ is the Nusselt number. h is the convective heat transfer coefficient. k is the thermal conductivity of the gas. Pr is the Prandtl number. $\theta_b = (1/A\bar{u})\int_A u\theta\,\mathrm{d}A$ is the bulk temperature of the gas. $\bar{M}$ is the cross-sectionally averaged Mach number.

The pressure and density are assumed uniform within any given cross-section of the channel. The validity of these and other approximations will be tested in § 5. We assume that the wall temperature of the conduit is uniform and equal to the temperature of the gas at the entrance. Owing to the small dimensions of our flow conduits and the high thermal conductivity of the silicon substrate, we also assumed that the flow is isothermal, $\theta = 1$. For the type of flows considered here, this is a very good approximation except, perhaps, when flow approaches choking conditions at the

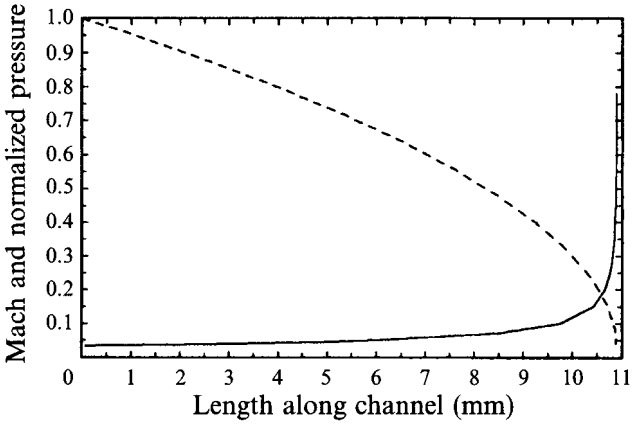

FIGURE 4. Pressure normalized by inlet pressure and Mach number versus axial position for isothermal nitrogen flow in channel JP9, $M_1 = 0.0337$. ——, Mach number; – – –, normalized pressure.

channel's exit. We verified this approximation in two ways. Using a Nusselt number and the Darcy friction factor for fully developed, incompressible flow, we integrated equation (1)–(4). For example, for flow in a 4.66 μm deep channel, at $Re = 305$ and $\bar{M} < 0.28$, the difference between the gas and wall temperatures was smaller than 1 °C (Harley 1993). Similar results were obtained by direct numerical simulations of the full Navier–Stokes equations (§5).

When choking occurs, however, an infinite amount of heat is required to maintain isothermal conditions. Since this is not realistic, it would be more appropriate to assume adiabatic flow in the vicinity of the choking point. For laminar, adiabatic, continuum flow, the chocking Mach number, $\overline{M_c} = \alpha^{-1/2}$. For example, for continuum flow between parallel plates, $\alpha = 54/35$ and $\overline{M_c} \sim 0.8$. Values of α for rectangular cross-sections of various aspect ratios are given in Harley (1993).

In most of our experiments, $\overline{M(x)} \ll \overline{M_c}$. Even when choking occurs, the isothermal approximation should not produce a significant error since along most of the channel's length, $\overline{M(x)} \ll \overline{M_c}$. $\overline{M(x)}$ approaches $\overline{M_c}$ only over a very short channel length as illustrated in figure 4, where the calculated, local $\overline{M(x)}$ is depicted as a function of x for isothermal flow in a 4.66 μm deep channel. Note that the flow accelerates from a modest $\bar{M} = 0.2$ to $\overline{M_c}$ within a distance of less than 0.25 mm. Given the smallness of the channel and the presence of axial conduction (neglected in (3)), a substantial deviation of θ from unity is unlikely.

In the experiments, we measured P_1, P_2, and $\bar{u}$. In order to estimate the friction factor, $\bar{f}$, averaged over the length of the conduit, we employ equation (2). To use this equation, we need to integrate the third term and to obtain an estimate for β. The integration of the third term requires knowledge of $\overline{u(x)}$, which we do not have. Fortunately, as we demonstrate later, this term is usually very small and can be neglected. To estimate β, knowledge of the axial velocity profile is required. To obtain such a profile, one frequently invokes the 'locally fully developed' approximation. In the next section, we derive an expression for such a 'fully developed' profile in continuum flow. Then, in §5, we verify the validity of the 'locally fully developed' approximation through comparison with numerical simulations.

4. The 'locally fully developed' velocity profile in continuum flow

Recently, van den Berg *et al.* (1993) derived a simple, 'locally fully developed' theory for low Mach number, compressible, isothermal flow in circular capillaries. In contrast, our experimental channels had a rectangular cross-section with, in most cases, a large ratio between the width and height. Because of this large ratio, we approximate our flow as a flow between two parallel plates spaced distance D apart.

For two-dimensional, constant viscosity, isothermal, compressible channel flow, the non-dimensional continuum and momentum equations are, respectively,

$$\frac{\partial(\rho u)}{\partial x} = 0 \tag{5}$$

and

$$\rho u \frac{\partial u}{\partial x} = -\frac{1}{\gamma}\frac{\mathrm{d}P}{\mathrm{d}x} + \frac{1}{G}(\tfrac{4}{3}+\phi)\frac{\partial^2 u}{\partial x^2} + \frac{1}{G}\frac{\partial^2 u}{\partial y^2}. \tag{6}$$

The boundary conditions are no-slip at solid walls and prescribed inlet and exit pressures,

$$u(x,-1) = u(x,1) = 0, \quad P(0) = 1, \quad P(L) = \delta. \tag{8}$$

In the above, we used the half-distance ($\frac{1}{2}D$) as the lengthscale. δ is the ratio between the exit and inlet pressures. Following Prud'homme *et al.* (1986) and van den Berg *et al.* (1993*a*, *b*), we assumed that the density and pressure are functions of x but not of y, and we neglected the transverse velocity component $v(x,y)$. The latter is a bald approximation which leads to an inconsistent mathematical model. Nevertheless, numerical calculations (§6) revealed that, for the type of flows considered here, even for relatively high subsonic Mach numbers, $\mathrm{Max}_{x,y}(v(x,y)/u(x,0)) < 10^{-2}$.

The axial velocity can be factored,

$$u(x,y) = u_m(x)\,E(y), \tag{9}$$

where $u_m(x)$ is the centreline velocity and $u_m(0) = 1$. Upon substituting (9) into (6) and using (4) to eliminate the pressure, we obtain:

$$-E^2(y)\frac{\mathrm{d}\ln(\rho)}{\mathrm{d}x} + \frac{(\frac{4}{3}+\kappa)}{G}\rho\frac{\mathrm{d}}{\mathrm{d}x}\left(\frac{1}{\rho^2}\frac{\mathrm{d}\rho}{\mathrm{d}x}\right)E(y) = -\frac{1}{2\gamma}\frac{\mathrm{d}\rho^2}{\mathrm{d}x} + \frac{1}{G}E''(y), \tag{10}$$

with

$$E(\pm 1) = 0, \quad \rho(0) = 1, \quad \rho(L) = \delta, \tag{11}$$

where the primes denote differentiation with respect to y.

Equation (10) will only be used to generate average relationships. In fact, this equation is mathematically inconsistent. Specification of different y values in (10) lead to different solutions for $\rho(x)$. For example, when $y = 1$, $\rho(x) = (1-(1-\delta^2)(x/L))^{1/2}$, which represents a balance between the pressure gradient and the wall shear stress.

Integration of equation (10) along the channel's length leads to a second-order differential equation for E,

$$C_1 E^2(y) - C_3 E(y) = 1 + C_2 E''(y), \quad E'(0) = E(1) = 0 \quad (0 \leqslant y \leqslant 1), \tag{12}$$

where the constants, $C_1 = -2\gamma L n(\delta)/(1-\delta^2)$ and $C_2 = 2\gamma L/(1-\delta^2)G$, depend only on boundary conditions. In contrast, the evaluation of the third constant, $C_3 = 2\gamma(\frac{4}{3}+\phi)Z/G(1-\delta^2)$, where $Z = \int_L^0 \rho\,(\mathrm{d}/\mathrm{d}x)((1/\rho^2)(\mathrm{d}\rho/\mathrm{d}x))\,\mathrm{d}x$, requires knowledge of $\rho(x)$, which can be obtained only by solving (10). Fortunately, as we show later, for the flows considered here, C_3 is extremely small and can be safely neglected. Below, we set $C_3 = 0$.

We solved equation (12) both numerically, using a shooting technique, and analytically. The closed form solution is:

$$\frac{(6C_2)^{1/2}}{(C_1(A_+ - E(0)))^{1/2}} F\left[\sinh^{-1}\left(\left(\frac{E(0)-E(y)}{E(y)-A_-}\right)^{1/2}\right)\middle|\frac{A_+ - A_-}{A_+ - E(0)}\right] = y, \tag{13}$$

where

$$A_\pm = -\tfrac{1}{2}E(0) \pm \left(\frac{\sqrt{3}}{2}\right)(4C_1^{-1} - E^2(0))^{1/2} \quad \text{and} \quad F[u\,|\,m] = \int_0^u \frac{1}{(1+m\sinh^2(\phi))^{1/2}}\,\mathrm{d}\phi$$

is an elliptic integral of the first kind with an imaginary argument. The elliptic function was evaluated with the aid of MATHEMATICA (Wolfram 1992).

For illustration purposes, we computed $E(y)$ as a function of y for nitrogen flow in a 4 μm deep and 400 μm long channel. For low ($M_1 = 0.07$, $M_2 = 0.15$, $\delta = 0.523$) and moderate ($M_1 = 0.22$, $M_2 = 0.84$, $\delta = 0.225$) Mach number flows, the difference between $E(y)/E(0)$ and the parabolic profile, $(1-y^2)$, was less than 0.3 % and 3 %, and $\{C_1, C_2, C_3\} = \{2.49, 6.3, 1.7\times10^{-3}\}$ and $\{4.39, 6.14, 1.2\times10^{-2}\}$, respectively. Note also that the nonlinear term's contribution in (12) is quite small (< 3 %). In the next section, we compare $E(y)$ with numerical results.

Once $E(y)$ is known, neglecting the second term in (10), which is consistent with setting $C_3 = 0$, we integrate (10) over the cross-section to obtain a momentum balance similar to (2),

$$\frac{1}{2\gamma}(\rho^2 - 1) - \overline{E^2}Ln(\rho) = G^{-1}E'(1)\,x \quad (0 \leqslant x \leqslant L). \tag{14}$$

We calculated $\rho(x)$ using this equation. The results are presented in the next section.

5. Numerical solution

We solve numerically, with the aid of the finite element program FIDAP, the two dimensional Navier–Stokes and energy equations for compressible flow of a gas between two isothermal, parallel plates. The boundary conditions used in the simulation consist of uniform inlet and exit pressures and a uniform inlet temperature equal to the walls' temperature. In all the simulations, $\phi = 0.6$, $Pr = 0.69$, $\gamma = 1.4$, and $L = 100$. The simulations correspond, for example, to nitrogen flow in a 4 μm deep channel with $T_1 = 373$ K and $P_2 = 0.1$ MPa. The results of the simulations were tested for self-consistency by grid refinement. Simulations with 300×27 and 500×33 grid points gave indistinguishable results.

For brevity, we report here only the results of two numerical simulations, a relatively low Mach number flow ($M_1 = 0.07$, $M_2 = 0.15$, $\delta = 0.523$, $Re_1 = 1.54$) and a moderate Mach number flow ($M_1 = 0.22$, $M_2 = 0.84$, $\delta = 0.225$, $Re_1 = 10.75$). The reported Mach numbers were evaluated at the channel's centreline.

5.1. *Low Mach number flow* ($M_1 = 0.07$, $M_2 = 0.15$, $\delta = 0.523$)

Figure 5 depicts the numerical (dots) and the theoretical predictions (solid lines) obtained in §4 for the centreline speed $u(x, 0)$, the centreline density $\rho(x, 0)$, and the wall shear stress as functions of the axial location x. All these quantities were normalized with the corresponding inlet conditions at $x = 0$. The difference between theoretical (§4) and numerical results was always smaller than 1 %.

Figure 5 also depicts the numerically computed centreline temperature as a function of x. The temperature drop along the channel's length is smaller than 0.5 %. This temperature drop results from expansion cooling. The relatively sharp temperature

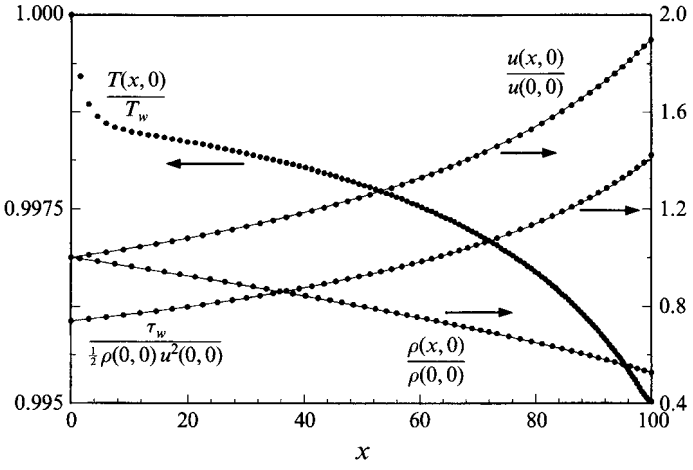

FIGURE 5. The centreline velocity, $u(x,0)$, centreline density $\rho(x,0)$, centreline temperature $T(x,0)$, and wall shear stress are depicted as functions of the axial coordinate x. ——, Analytical and ●, numerical results for $M_1 = 0.07$, $M_2 = 0.15$ and $\delta = 0.523$.

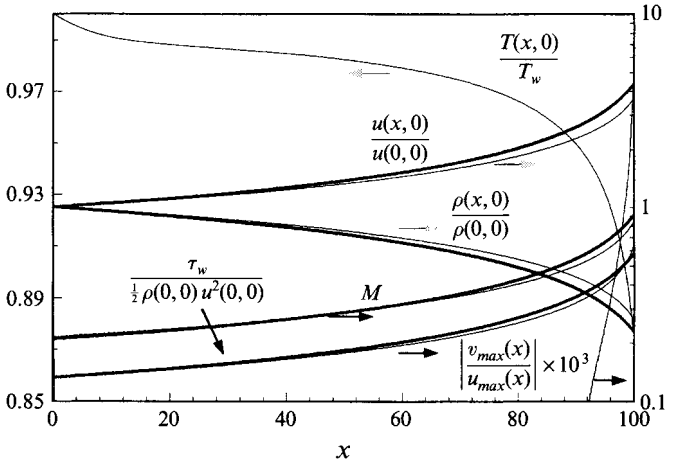

FIGURE 6. The centreline velocity, $u(x,0)$, the centreline density $\rho(x,0)$, the centreline temperature $T(x,0)$, the centreline Mach number, $M(x)$, the maximum value of the transverse velocity, and the wall shear stress are depicted as functions of the axial coordinate x. ——, analytical and ——, numerical results for $M_1 = 0.21$, $M_2 = 0.85$ and $\delta = 0.225$.

drop next to the entrance is necessary to provide a conductive path for transporting energy from the wall into the gas. This sharp drop in temperature was also predicted theoretically (van den Berg 1993*b*).

The analytical, numerical, and parabolic axial velocity profiles (not depicted here) agreed with each other within 0.3%.

5.2. *Moderate Mach number flow* ($M_1 = 0.22$, $M_2 = 0.84$, $\delta = 0.225$)

Figure 6 depicts the numerical (thin lines) and theoretical (heavy lines) values of the centreline velocity, centreline Mach number, centreline density, and wall shear stress as functions of x. Additionally, the figure also depicts the numerical results for the centreline temperature and $\mathrm{Max}_y(v(x,y)/u(x,0))$ as functions of x. Even for the relatively high subsonic Mach numbers, the numerical results were in reasonable

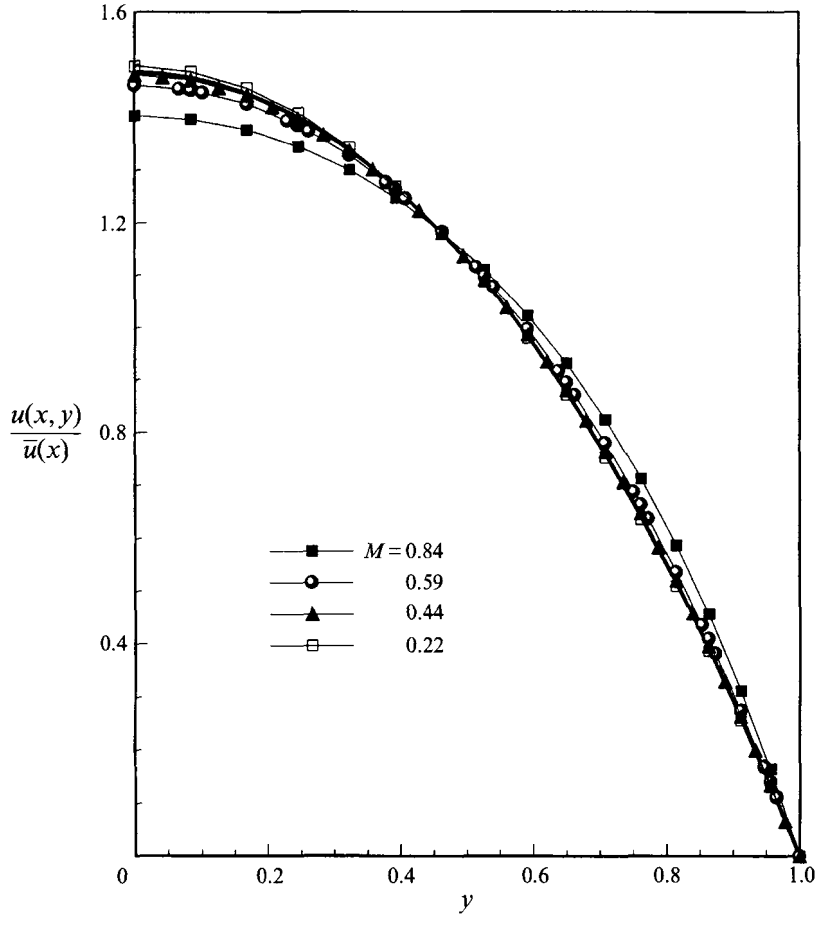

FIGURE 7. The axial velocity, normalized with the cross-sectionally averaged velocity, is depicted as a function of y for centreline Mach numbers, $M = 0.22$, 0.44, 0.59 and 0.84. The various symbols denote numerical results. The solid line represents the analytical prediction, $E(y)$.

agreement with theoretical predictions. The discrepancy between the theoretical wall shear stress and the numerical one was smaller than 3% when $M < 0.3$ and increased to about 10% next to the channel's exit. The centreline temperature decreased by as much as 12% along the channel's length with most of the drop occurring next to the channel's exit. The transverse velocity was always smaller than 0.7% of the centreline axial velocity.

Figure 7 depicts the normalized velocity profile $u(x,y)/\overline{u(x)}$ as a function of y for $M = 0.22$, 0.44, 0.59 and 0.84. The solid line represents $E(y)/\bar{E}$ which is independent of x and depends only on the inlet and exit conditions. As the Mach number increases, the numerically computed profile flattens a bit, and its peak velocity is smaller than the approximate, analytical prediction.

Figure 8 depicts the transverse velocity profile $v(x,y)/v_{max}(x)$ as a function of y for $M = 0.44$, 0.50, 0.59 and 0.75. The transverse velocity facilitates mass transport from the wall's region towards the channel's centre. Owing to symmetry, $v(x,0) = 0$. At the impermeable wall, the velocity is again zero. According to the continuity equation, $(\partial(\rho v)/\partial y)_{y=1} = 0$. Since $\rho \sim \rho(x)$, we also have $(\partial v/\partial y)_{y=1} \sim 0$, which is evident in figure 8.

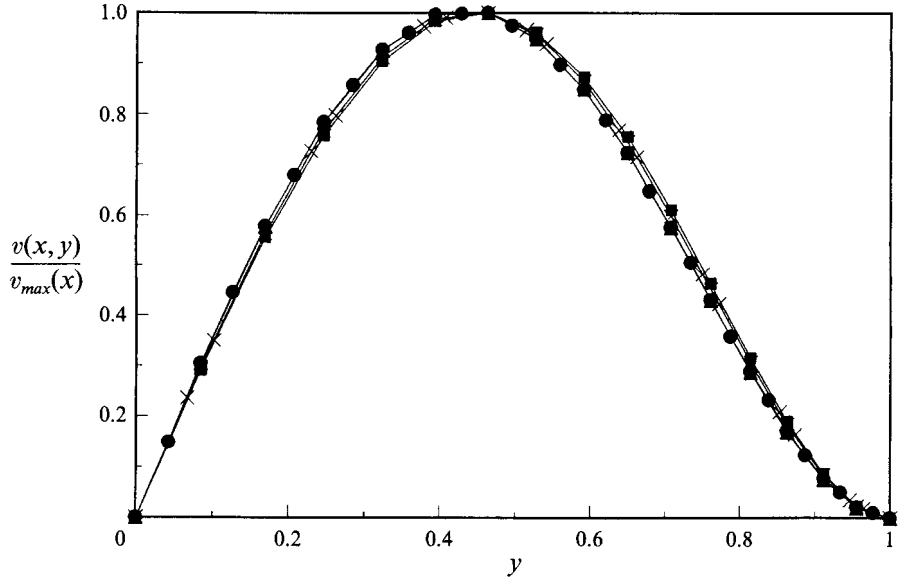

FIGURE 8. The transverse velocity, normalized with the centreline axial velocity, is depicted as a function of y for ●, $M = 0.44$; ▲, 0.50; ×, 0.59; ■, 0.74.

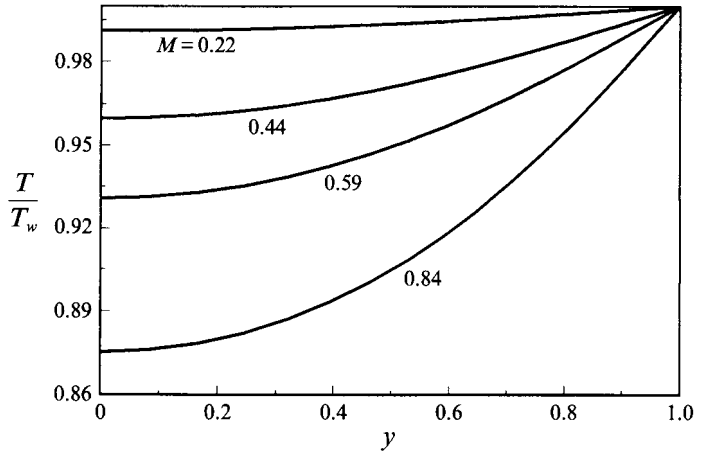

FIGURE 9. The temperature is depicted as a function of y for $M = 0.22$, 0.44, 0.59 and 0.84.

Figures 9 and 10 depict the temperature and pressure profiles as functions of y for $M = 0.22$, 0.44, 0.59 and 0.84. The temperature assumes its minimum value at the channel's centre. The difference between the centreline and wall temperatures increases as the Mach number increases.

Figure 10 illustrates that the pressure is almost uniform at each cross-section. Thus, the approximation of $p(x, y) \sim p(x)$ is a very good one.

We also calculated at $y = 0.5$, the relative magnitude of the term we neglected in equation (6), $v(\partial u/\partial y)/u(\partial u/\partial x)$, as a function of x; and we found it to be always smaller than 3%.

In summary, the numerical work supports the assumptions that the transverse velocity can be neglected and that the pressure and density may be assumed uniform in any cross-section. For the type of flows considered here, one can reasonably employ the 'locally fully developed' approximation when one interprets the experimental data.

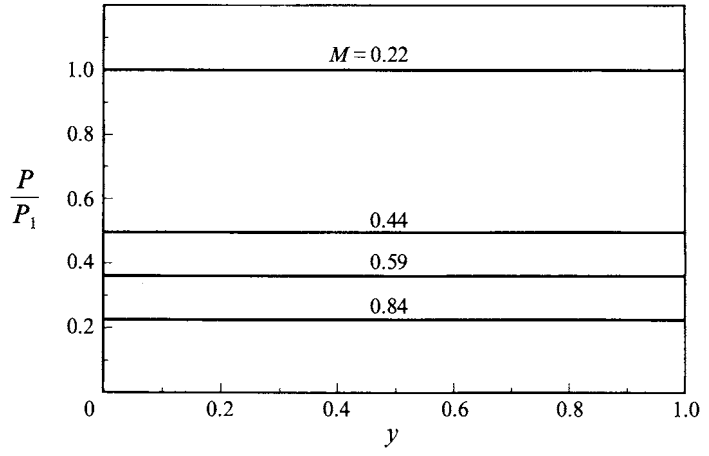

FIGURE 10. The pressure is depicted as a function of y for $M = 0.22$, 0.44, 0.59 and 0.84.

6. Working equations for the interpretation of the experimental data

In this section, we use the 'locally fully developed' approximation to obtain the working equations we will use in the processing of our experimental data. We simplify matters a bit by taking advantage of the fact that for the flows investigated here, the nonlinear term in (12) is small. Hence, the fully developed assumption implies that the velocity profile can be determined by solving,

$$\mu \nabla^2 u = \frac{\mathrm{d}P}{\mathrm{d}x}, \tag{15}$$

with the wall boundary condition,

$$u_w = -\kappa Kn \left(\frac{\partial u}{\partial n}\right)_w. \tag{16}$$

For continuum flow, $Kn \to 0$, equation (16) reduces to the familiar no-slip condition. For rarefied flow, Kn is a function of x. In the above, ∇^2 is a two-dimensional Laplace operator in the conduit's cross-section, $Kn = \lambda/D$ is the Knudsen number, D is the channel depth, $\lambda = \mu\pi^{1/2}/\rho(2RT)^{1/2}$ is the mean free path, R is the ideal gas constant, n is a non-dimensional coordinate perpendicular to the solid surface which has been normalized by the channel depth, and subscript w indicates that the variable is evaluated at the conduit's wall.

Maxwell showed that $\kappa = \kappa_0(2-\xi)/\xi$, where κ_0 is a constant of $O(1)$ and $0 < \xi < 1$ is the fraction of the molecule's tangential momentum lost through collisions with the solid surface. In general, κ may depend on the surface's roughness and temperature and the gas type. Albertoni, Cercignani & Gotusso (1963) calculated $\kappa = 1.1466$ by solving the linearized Boltzmann equation. For $Kn < 0.05$, Sreekanth (1968) obtained a better agreement between his experimental data and theory using $\kappa = 1$ rather than the calculated value of 1.1466. Kennard (1938) reports empirical values for κ ranging from 1 to 1.5 for various gas and surface combinations.

Solutions of equations (15)–(16) for rectangular and circular cross-sections are available in Ebert & Sparrow (1965) and Sreekanth (1968). For example, for flow between parallel plates (Harley 1991),

$$\frac{u(y)}{\bar{u}} = \frac{1-4y^2+4\kappa Kn}{\frac{2}{3}+4\kappa Kn} \quad (-\tfrac{1}{2} \leqslant y \leqslant \tfrac{1}{2}) \tag{17}$$

and
$$\beta = \frac{(1+4\kappa Kn)(\frac{1}{3}+4\kappa Kn)+\frac{1}{5}}{(\frac{2}{3}+4\kappa Kn)^2}. \tag{18}$$

For rarefied flow, β, like Kn, is a function of x. For continuum flow ($Kn \to 0$) between parallel plates, $\beta = 1.2$.

We present our experimental results in terms of the Poiseuille number, $Po(Kn) = fRe$. For locally fully developed, rarefied flow, at any x location, the ratio between the rarefied and the continuum Poiseuille numbers is:

$$\frac{Po(Kn)}{Po(0)} = \frac{1}{1+\eta\kappa Kn}, \tag{19}$$

where $Po(0)$ and η are constants which depend on channel geometry only and are independent of Kn. For example, for flow between parallel plates, $Po(0) = 96$ and $\eta = 6$. Ebert & Sparrow (1965) and Shah & London (1978) document, respectively, values of η and $Po(0)$ for various cross-sectional geometries.

In our experimental work, we measured the inlet and outlet pressures and temperatures as well as the flow rate. The average Poiseuille number along the channel's length (Ebert & Sparrow 1965),

$$\overline{Po}(Kn_1) = -\frac{D_H}{\epsilon\, Re\, L}\left\{\left[\left(\frac{P_2}{P_1}\right)^2 - 1\right] + 2\eta\kappa Kn_1\left(\frac{P_2}{P_1} - 1\right) + 2\epsilon\beta\, Re^2\left[\eta\kappa Kn_1\left(\frac{P_1}{P_2} - 1\right) - Ln\left(\frac{P_2}{P_1}\right)\right]\right\}, \tag{20}$$

was obtained by integrating equations (1) and (2) with β = constant and Kn varying as a function of pressure. Sreekanth (1968) showed that the approximation β = constant had little effect on the magnitude of $\overline{Po}$ since β is a weak function of Kn. In equation (20), $\epsilon = \mu^2 RT/P_1^2 D_H^2$.

We used (20) to process our experimental data. The Reynolds number was evaluated at the inlet temperature. When no choking occurred, P_2 was the pressure measured at the channel's exit. When choking occurred, we computed P_2 from the equation,

$$Ln\left(\frac{p_2}{p_1}\right) = -Ln\left(\frac{Mc}{M_1}\right)(1+\chi(M_1)), \tag{21}$$

where $\chi(M_1) = 0$ for isothermal flow.

In order to estimate the magnitude of the error caused by assuming isothermal flow in the choked channel, we also calculated P_2 assuming adiabatic flow. In this case,

$$\chi(M_1) = \frac{Ln((1+\frac{1}{2}(\gamma-1)\alpha Mc^2)/(1+\frac{1}{2}(\gamma-1)\alpha M_1^2))}{Ln(Mc^2/M_1^2)}.$$

For small entrance Mach numbers ($M_1 < 0.1$, which was the case in most of our experiments), the differences between the isothermal and adiabatic calculations of P_2 and $\overline{Po(0)}$ were less than 9% and 0.1%, respectively. The weak dependence of $\overline{Po(0)}$ on P_2 is due to the fact that $P_1 \gg P_2$ for all the experiments in which choked flow occurred.

7. Results and discussion

Experimental investigations were conducted using the eight different flow channels documented in table 1 and three different gases: nitrogen, helium, and argon. Most of the experimental data (figures 11, 12 and 14) are presented in terms of the reduced

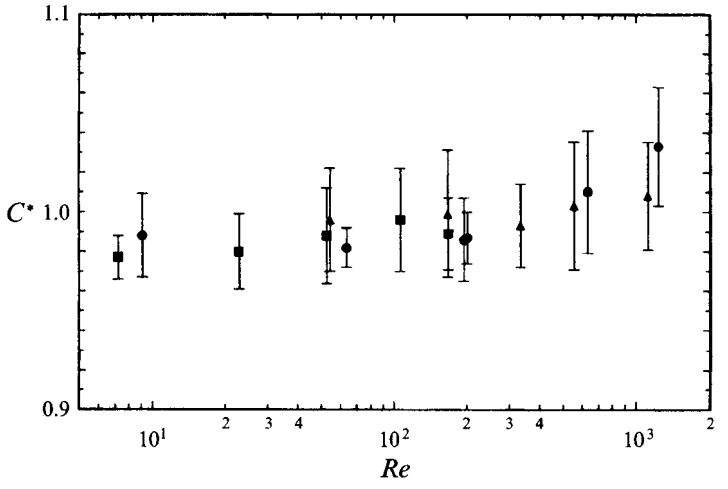

FIGURE 11. C^* is depicted as a function of the Reynolds number for ●, nitrogen; ■, helium; and ▲, argon flow in a 11.04 μm deep channel (JP3).

Poiseuille number, $C^* = (Po)_{experiment}/(Po)_{theory}$. $C^* \equiv 1$ when the measured friction factor is equal to theoretical predictions. Each point in figures 11, 12 and 14 represents the average of twenty measurements, and the vertical bars denote two standard deviations.

Figure 11 depicts C^* as a function of Re for a 11.04 μm deep channel (JP3). C^* was calculated using equation (20) with $Kn_1 = 0$. The inlet pressure ranged from 0.2 MPa to 2.1 MPa. The exit pressure was atmospheric. The exit Mach number ranged from $M_2 = 0.02$ to choked flow. The Knudsen number ranged from 0.017 to 2.75×10^{-4}, which corresponds to continuum flow. The magnitude of C^* decreases slightly from 1.03 to 0.98 as Re decreases from 1200 to 5. This decrease in C^* can be attributed to the diminishing effect of the development length. For $Re = 1200$, the estimated developing length may extend up to 10% of the channel's length. Overall, the average friction constant was within 3% of the theoretical value for fully developed, incompressible flow.

Figure 12 depicts C^* as functions of Re for a 0.51 μm deep channel (JH6). The dashed and solid lines correspond, respectively, to C^* values calculated using equation (20) with $Kn_1 = 0$ and with $Kn_1 > 0$. The inlet pressure ranged from 1.1 MPa to 3.4 MPa. The exit pressure was atmospheric. The exit Mach number ranged from 0.0014 to 0.0189. C^*, calculated using the non-slip boundary condition ($Kn_1 = 0$, dashed line), decreased from 0.98 to 0.82 as Re decreased from 0.43 to 0.012. Owing to the small dimensions of this channel and the low Re numbers encountered, the effects of the development length were negligibly small and cannot account for this decrease. In contrast, Kn ranged from 0.004 to 0.373 which suggests transitional flow. Thus, we attribute the reduction in C^* to wall slip. This effect is most pronounced at low Re since low Re corresponds to a relatively low average pressure in the channel, which in turn implies a relatively high Knudsen number and significant wall slip. For example, for $Re = 0.012$, the inlet and outlet Knudsen numbers were, respectively, 0.025 and 0.373.

Next, we examine whether wall slip can, in fact, explain the experimental observations. Using equation (20) with $Kn_1 > 0$ and $\kappa = 1$, we calculate C^* (solid line in figure 12) as a function of Re. The flat behaviour of the solid curve in figure 12 indicates that the data is successfully predicted by an isothermal, locally fully

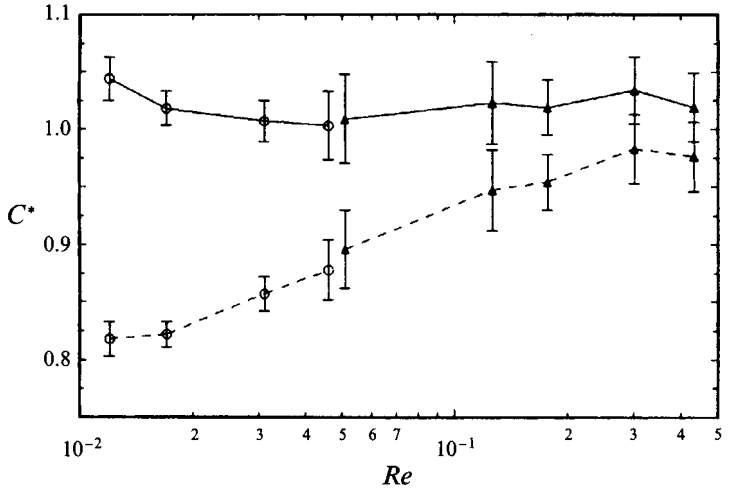

FIGURE 12. C^* values calculated with ---, a non-slip and ——, a slip boundary condition are depicted as functions of Re for ▲, nitrogen and ○, helium flow in a 0.51 μm deep channel (JH6).

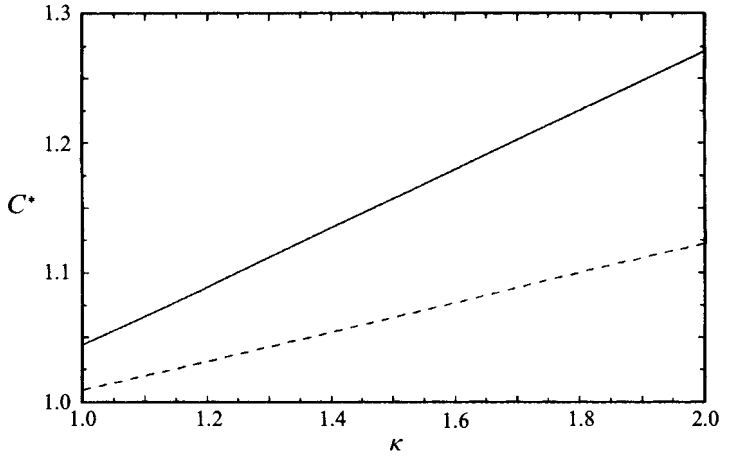

FIGURE 13. C^* is depicted as a function of κ for ——, helium ($Re = 0.012$) and ---, nitrogen ($Re = 0.051$) flow in a 0.51 μm deep channel (JH6).

developed, single coefficient wall-slip model. Like Sreekanth (1968), we obtained a better agreement between experiments and theory when we used $\kappa = 1$ rather than the $\kappa = 1.1466$ calculated by Albertoni *et al.* (1963). The sensitivity of our results to the particular choice of κ is illustrated in figure 13, where we depict C^* ($Kn_1 > 0$) as a function of κ for nitrogen ($Re = 0.051$) and helium ($Re = 0.012$) flows in the 0.51 μm deep channel.

In figure 14, we depict C^* ($Kn_1 > 0$ and $\kappa = 1$) for nitrogen, helium, and argon gas flow as a function of the channel's hydraulic diameter for all the channels used in our experiments. In order to obtain figure 14, we generated plots (not shown here) similar to those of figures 11 and 12 for each of the channels. In the deeper channels, in which rarefaction effects were deemed unimportant and the development length exceeded 1 % of the channel length, we extrapolated the C^* data to zero Re in order to eliminate the effects of the development length. In the shallower channels, in which no development

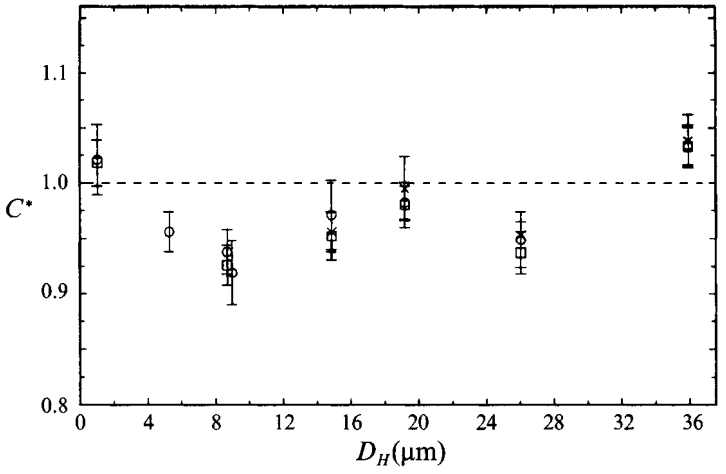

FIGURE 14. C^* is depicted as a function of the hydraulic diameter, D_H, for ○, nitrogen; □, helium; and ×, argon gas flow.

	Knudsen number, *Kn*			
	Nitrogen		Helium	
Channel	At the inlet	At the outlet	At the inlet	At the outlet
JH10	0.003	0.014	—	—
JP9	0.002	0.014	0.004	0.041
V3	0.002	0.023	—	—
JH6	0.012	0.129	0.025	0.363

TABLE 2. Maximum exit Knudsen numbers for nitrogen and helium flow in channels JH10, JP9, V3 and JH6

length effects were detected but rarefaction effects were important, C^* represents an average of the experimental data for all *Re* numbers encountered. The inlet and outlet *Kn* numbers encountered for the lowest *Re* number flow in the shallow channels are documented in table 2. All the experimental data is within 8% of theoretical predictions based on the isothermal, locally fully developed, single coefficient slip model.

8. Conclusions

Experimental and theoretical investigations of subsonic, compressible flow in microsize, long conduits were conducted. The numerical simulations indicated that the pressure may be assumed to be uniform in the conduit cross-sections perpendicular to the direction of the flow and that the transverse velocity can be neglected. Consequently, the 'locally fully developed' approximation leads to predictions which are in reasonable agreement with those resulting from numerical simulations of the full Navier–Stokes equations and with experimental observations.

In all our experiments, the Knudsen number was less than 0.38 and the data were within 8% of theoretical predictions of the friction constant based on isothermal,

locally, fully developed flow and incorporating a single coefficient wall-slip model. This is well within our experimental uncertainty of 12%. This observation is consistent with results obtained by other experimenters (i.e. Sreekanth 1968) who have examined compressible flow in much larger channels.

J.C.H. gratefully acknowledges support by NASA grant no. NGT-50688. Y.H. was supported by a grant from the Hewlett-Packard Corporation, Little Falls Site, and H.H.B. and J.N.L. were supported, in part, by the NSF through grant EET88-15284. Professor R. Warrington, Jr, of Louisiana Tech University, provided us with the surface profile shown in figure 3.

REFERENCES

ALBERTONI, S., CERCIGNANI, C. & GOTUSSO, L. 1963 Numerical evaluation of the slip coefficient. *Phys. Fluids* **6**, 993–996.

BERG, H. R. VAN DEN, SELDAM, C. A. TEN & GULIK, P. S. VAN DER 1993*a* Compressible laminar flow in a capillary. *J. Fluid Mech.* **246**, 1–20.

BERG, H. R. VAN DEN, SELDAM, C. A. TEN & GULIK, P. S. VAN DER 1993*b* Thermal effects in compressible viscous flow in a capillary. *Intl J. Thermophys.* **14**, 865–892.

CHOI, S. B., BARRON, R. F. & WARRINGTON, R. O. 1991 Fluid flow and heat transfer in microtubes. In *Symposium on Micromechanical Sensors, Actuators, and Systems* (ed. D. Cho, R. Warrington Jr, A. Pisano, H. H. Bau, C. Friedrich, J. Jara-Almonte & J. Liburdy), *ASME DSC* **32**, 123–134.

EBERT, W. A. & SPARROW, E. M. 1965 Slip flow in rectangular and annular ducts. *Trans ASME* D: *Journal Basic Engng* **87**, 1018–1024.

HARLEY, J. C. 1991 *Compressible gas flow in micron and submicron sized channels.* MS thesis, Department of Mechanical Engineering and Applied Mechanics, University of Pennsylvania.

HARLEY, J. C. 1993 *Compressible gas flow in microchannels and microjets.* PhD thesis, Department of Mechanical Engineering and Applied Mechanics, University of Pennsylvania.

JAEGER, R. C. 1988 *Introduction to Microelectronic Fabrication*, vol. 5. Modular Series on Solid State Devices (ed. G. Neudeck & R. Pierret). Addison-Wesley.

JOYCE, J. W. 1983 Fluidics: basic components and applications. *US Army Electronics Development Command, Harry Diamond Labs Special Report* HDL-SR-83-9.

KEENAN, J. H. & NEUMANN, E. P. 1946 Measurements of friction in a pipe for subsonic and supersonic flow of air. *J. Appl. Mech.* **13** (2), A-91–A-100.

KENNARD, E. H. 1938 *Kinetic Theory of Gases.* McGraw-Hill.

PFAHLER, J., HARLEY, J., BAU, H. & ZEMEL, J. 1991 Gas and liquid flow in small channels. *Symp. Micromechanical Sensors, Actuators, and Systems* (ed. D. Cho, R. Warrington Jr, A. Pisano, H. Bau, C. Friedrich, J. Jara-Almonte & J. Liburdy), *ASME DSC* **32**, 49–60.

PRUD'HOMME, R. K., CHAPMAN, T. W. & BOWEN, J. R. 1986 Laminar compressible flow in a tube. *Appl. Sci. Res.* **43**, 67–74.

SHAH, R. K. & LONDON, A. L. 1978 *Laminar Flow Forced Convection in Ducts.* Academic.

SHAPIRO, A. K. 1953 *The Dynamics and Thermodynamics of Compressible Fluid Flow*, vols 1 and 2. John Wiley.

SHAPIRO, A. H. & HAWTHORNE, W. R. 1947 The mechanics and thermodynamics of steady, one-dimensional gas flow. *J. Appl. Mech.* **14**, (4), A-317–A-336.

SREEKANTH, A. K. 1968 Slip flow through long circular tubes. *Rarefied Gas Dynamics* (ed. L. Trilling & H. Y. Wachman). Academic Press.

TERRY, S., JERMAN, J. & ANGELL, J. 1979 A gas chromatographic air analyzer fabricated on a silicon wafer. *IEEE Trans. Electron Devices*, ED-26, no. 12, 1880–1886.

TOULOUKIAN, Y. S., SAXENA, S. C. & HESTERMANS, P. 1975 *Thermophysical Properties of Matter*, vol. 11, IFI/Plenum.

TUCKERMAN, D. B. 1984 Heat transfer microstructures for integrated circuits. PhD thesis, Department of Electrical Engineering, Stanford University. Also report UCRL 53515, Lawrence Livermore National Laboratory.

WALLIS, G. 1970 Direct-current polarization during field-assisted glass–metal sealing. *J. Am. Ceramic Soc.* **53**, 563–567.

WU, P. & LITTLE, W. A. 1983 Measurement of friction factors for the flow of gases in very fine channels used for microminiature Joule–Thomson refrigerators. *Cryogenics*, May, 273–278.